Research Article

Zhaoshuai Li, Guxia Wang*, Jun Yan, Yongqiang Qian, Shengwei Guo, Yuan Liu, and Dan Li*

Value-added utilization of coal fly ash and recycled polyvinyl chloride in door or window sub-frame composites

https://doi.org/10.1515/gps-2023-0002 received August 18, 2022; accepted December 02, 2022

Abstract: Comprehensive utilization of coal fly ashes (CFA) solid waste is a worldwide urgent issue. In China, tens of millions of tons of CFA are un-utilized and stored or discarded in landfills per year, causing a significant waste of resources and a serious environmental hazard. Herein, we developed a new process to reuse CFA and recycled polyvinyl chloride (r-PVC) to produce door or window sub-frame (DWSF) composite materials, realized CFA and r-PVC trash to treasure. In this process, aluminate-modified CFA mixing with r-PVC and other additives obtain a mixture, subsequently extruding into pellets, re-extrusion, cooling, shaping, hauling, and cutting to DWSF materials. The mechanical properties of these are excellent and meet the National Standards, with static

bending and tensile strengths of 33 and 13.6 MPa, respectively, and a hardness of 89.2 HRR. Compared with the traditional CaCO₃-based DWSF, our CFA-based DWSFs have higher competitive both from the perspective of "carbon neutrality" and production costs. More strikingly, this process is simple, robust, and easy to industrialize, which allows large-scale, value-added utilization of CFA.

Keywords: coal fly ash, recycled polyvinyl chloride, door or window sub-frame, carbon neutrality

1 Introduction

Coal fly ash (CFA) is a powder-like solid waste captured from effluent gas released from coal combustion in coalfired thermal power plants [1]. The chemical composition of CFA is highly complex but primarily consists of SiO₂, Al_2O_3 , Fe_2O_3 , CaO, MgO, and Na₂O [2–4]. China is the world's largest coal consumer, and coal accounts for more than 60% of its energy consumption [5-10]. The combustion of four tons of coal produces one ton of CFA, resulting in CFA becoming one of the major solid wastes generated in China [11-13]. However, because of its low utilization (approximately 70%), the total cumulative stockpile of CFA has exceeded three billion tons [1]. CFA contains multiple heavy metals, and improper disposal not only wastes land resources but also causes significant environmental pollution [7,8,14–18]. Besides, regional imbalance between supply and demand is a primary problem hindering the recycling of CFA [1,19-21]. Therefore, increasing the utilization of CFA, and turning CFA waste into high value-added materials is one of urgent scientific issues in China, especially in its northwestern region [22,23].

The Chinese government has been vigorously improving the resource utilization of CFA in various fields. In the past few decades, CFA is predominantly used in road paving, mine backfill, cement mixtures, concrete, and low-end

Zhaoshuai Li: Ningxia Key Laboratory of Solar Chemical Conversion Technology, North Minzu University, Yinchuan 750021, China; Key Laboratory for Chemical Engineering and Technology, State Ethnic Affairs Commission, North Minzu University, Yinchuan 750021, China

Jun Yan, Yongqiang Qian: School of Materials Science and Engineering, North Minzu University, Yinchuan 750021, China Shengwei Guo: School of Materials Science and Engineering, North Minzu University, Yinchuan 750021, China; International Scientific and Technological Cooperation Base of Industrial Solid Waste Cyclic Utilization and Advanced Materials, Yinchuan 750021, China Yuan Liu: School of Materials Science and Engineering, North Minzu University, Yinchuan 750021, China; Polymer Research Institute of Sichuan University, The State Key Laboratory of Polymer Materials Engineering, Chengdu 610065, China

^{*} Corresponding author: Guxia Wang, Ningxia Key Laboratory of Solar Chemical Conversion Technology, North Minzu University, Yinchuan 750021, China; Key Laboratory for Chemical Engineering and Technology, State Ethnic Affairs Commission, North Minzu University, Yinchuan 750021, China, e-mail: guxia511@163.com

^{*} Corresponding author: Dan Li, School of Materials Science and Engineering, North Minzu University, Yinchuan 750021, China; International Scientific and Technological Cooperation Base of Industrial Solid Waste Cyclic Utilization and Advanced Materials, Yinchuan 750021, China, e-mail: lidan@nun.edu.cn

construction materials. Used as cement additive, concrete additive, and building materials accounts for 38%, 14%, and 26%, respectively [24-30]. CFA-based hollow building blocks [31], permeable bricks [32], and thermal insulation panels [33] are highly popular in China because of their ease of production and low cost. In recent years, CFA has been used in numerous new areas that have garnered attention from the academic and industrial communities; for example, it has been used as a composite electrolyte in CFA/polymer all-solid-state lithium batteries [5], a solid adsorbent for hydrogen storage [34], an enhancer in the dechlorination of polyvinyl chloride (PVC) [35], and as a broadband microwave absorber [36] as well as for agricultural improvement, wastewater treatment, and synthesisbased geopolymers with high compressive strength [37]. In addition, CFA has been used to prepare polymer composites [38], such as poly (ethylene terephthalate) composites [39,40], jute epoxy composites, high-density polyethylene composites [41], and PVC [42]. These CFA-plastic composites have not been successfully commercialized, and the CFA consumption is very limited. Therefore, to continue to improve the utilization of CFA, and realize CFA-based composites to commercial product remains challenging.

PVC is a common plastic material widely used in all aspects because of its excellent properties, most notably in window profiles' field. The process of PVC window profiles extrusion involves large amounts of "startup" and "shutdown" waste products. These waste materials often lead to an extreme waste of resources and an increase in production costs. In addition, CaCO₃ as filler constitutes more than 50% in PVC window profiles. Using large amounts of CaCO₃ causes CaCO₃ industry to be one of the largest carbon emission industries in China. CFA has low specific weight and high mechanical strength [43–45], and as a promising candidate filler replaces much more expensive CaCO₃ for the preparation of PVC composites.

In this article, we developed a new process for largescale consumption of CFA as filler to produce a new building material, namely door or window sub-frame (DWSF). This process promising for high value-added utilization of CFA and recycled PVC (r-PVC) is described as follows: the "startup" and "shutdown" waste products

of PVC window profiles are crushed into granules to obtain r-PVC materials. Subsequently, the granular r-PVC is blended with CFA, aluminate, and other additives by hot-mixing to prepare composite mixture. In the hotmixing process, the CFA is modified in situ by aluminate coupling agent and displays a good compatibility with the r-PVC resin. The mixture is then extruded into pellets, and subsequently re-extrusion, cooling, shaping, hauling, and cutting to DWSF materials. Compared with the conventional CaCO3-based DWSF (PVC/CaCO3 composites), the CFA-based DWSF (r-PVC/CFA composites) also exhibits high thermal stability, good mechanical properties, and waterproof performance. From the "carbon neutrality" perspective, this new process consumes CFA on a large scale, which saves a considerable amount of CaCO₃. Moreover, the obtained DWSF products can sell for up to 10,000 yuan per ton and using CFA to replace CaCO₃ as a filler reduces the production cost of DWSF by 20-35%. In brief, our research provides an effective approach for the large-scale and high value-added utilization of CFA.

2 Experimental section

2.1 Materials

CFA was purchased from a local coal-fired power plant in Ningxia, China. Table 1 summarizes the chemical composition of the CFA. As shown, SiO₂ and Al₂O₃ are the main components of the CFA, collectively comprising 67.8% of the dry weight of the CFA. In addition, the CFA contains Fe (Fe₂O₃), Ca (CaO), Mg (MgO), K (K₂O), Na (Na₂O), Ti, and P in large amounts, and the CFA's loss on ignition is 5.52%. The CFA was used as received without any additional treatments. r-PVC was purchased from Yinchuan Building Materials Co., Ltd, of the Ningxia Shide Group. Ca–Zn stabilizer (WS208-C10) used as heat stabilizer for PVC was purchased from Guangzhou Warm Plastic Additives Co., Ltd. Chlorinated polyethylene (CPE135) flexibilizer was purchased from Weihai Hisea Plastic Rubber Co., Ltd. Impact modifier of acrylics (ACR, LP-812) was

Table 1: Elemental analysis of CFA*

Elements	SiO ₂	Al ₂ O ₃	Fe ₂ O ₃	CaO	K ₂ O	MgO	Na ₂ O	Ti	P
Content (%)	44.28	23.66	4.3	2.61	1.1	0.78	0.5	0.691	0.102

^{*}Determined using X-ray fluorescence spectroscopy.

purchased from Shandong Ruifeng Chemical Co., Ltd. Polyethylene (PE) wax used as a lubricating agent was purchased from Qingdao Sainuo New Material Co., Ltd. Aluminate coupling agent (JW411) was purchased from Nanjing Jingtianwei Chemical Co., Ltd. All materials and chemicals were used as received.

An FM1000 hot mixer and an HM3500 cold mixer (Henschel Industrietechnik GmbH), as well as a KMD90-26 extruder and a KMD114-32 extruder (KraussMaffei) were used in the experiments.

2.2 CFA-based DWSF composites preparation

Following the preparation process shown in Figure 1, the required amounts of r-PVC, CFA, Ca-Zn stabilizer, CPE, ACR, and PE wax (Table 2) were weighed out and added through a connecting tube into a high-speed mixer. Thereafter, they were hot-mixed at 118°C and 600–800 rpm for 5–10 min (the temperature was approximately 118°C) to remove the moisture from the CFA. Subsequently, the required amount of the aluminate coupling agent was weighed out and added into the mixture via a conveyor belt. The blending process was continued for another

Table 2: Recipes of traditional and new DWSF composites

Recipe of traditional DWSF (PVC/CaCO ₃ composites)							
PVC	Ca–Zn stabilizer	CPE	ACR	Light CaCO₃	Heavy CaCO ₃	Stearic acid	
100	4.2	10	0.9	48	28	0.8	

r-PVC	Ca-Zn stabilizer	СРЕ	ACR	CFA	PE wax	Aluminate
100	1.3	5	0.8	40	0.3	0.6
100	1.3	5	0.8	60	0.3	0.9
100	1.3	5	0.8	80	0.3	1.2
100	1.3	5	0.8	100	0.3	1.5

Units: parts per hundred parts of resin, abbreviated as phr.

5 min, thus yielding the modified CFA. Immediately afterward, the mixture was transferred to a cold mixer for cold mixing at 46°C for 5-10 min. After this process was completed, a dry mixture was obtained.

The dry mixture was added into the hopper of a parallel twin-screw extruder for melt blending. The rotational speeds of the screws in the parallel twin-screw extruder and dosing unit were set to 8 and 28.5 rpm, respectively. The sectional temperatures of the extruder barrel were set to 176°C, 176°C, 176°C, 176°C, 172°C, and

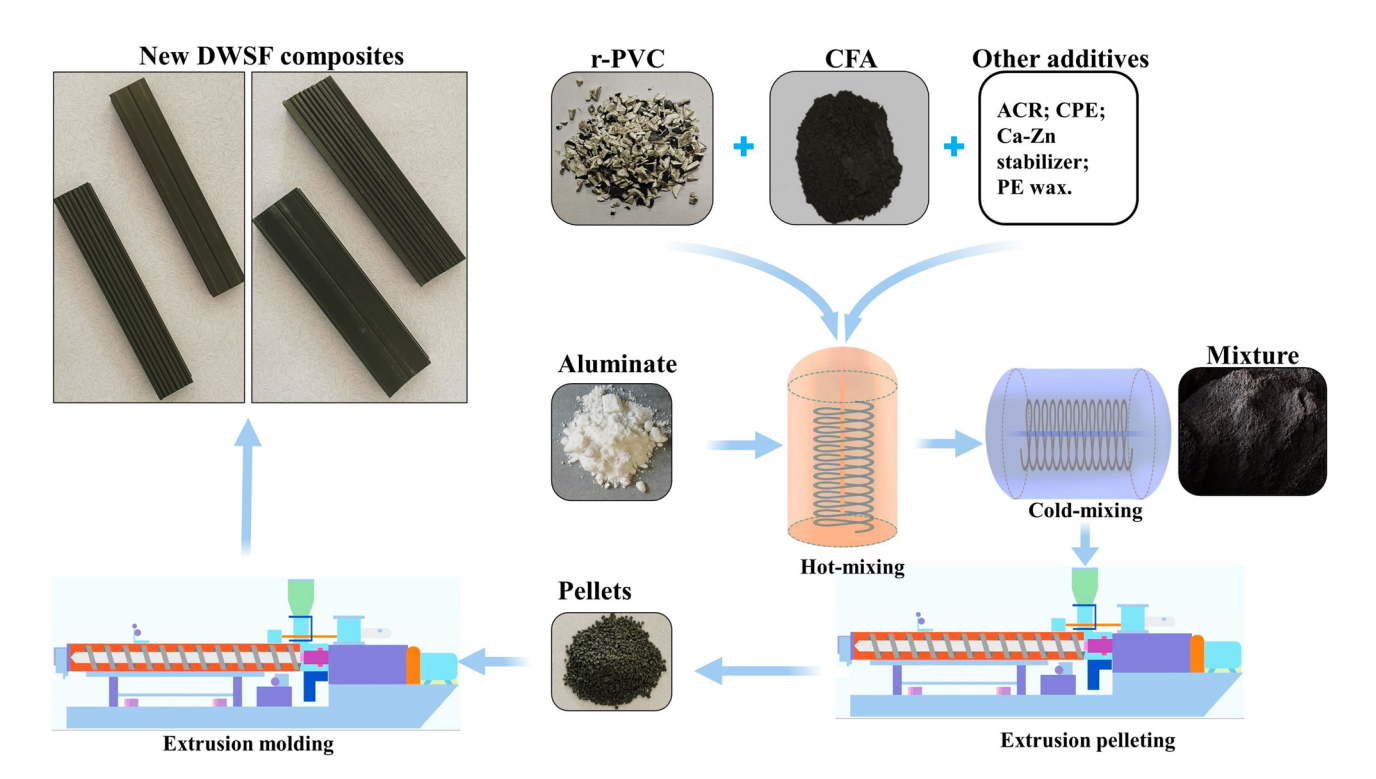


Figure 1: Process flow diagram of the preparation of CFA-based new DWSF composites.

172°C. The sectional temperatures of the connecting area were set to 170°C and 170°C, and the pressure and temperature of the melt were 5.7 MPa and 181°C, respectively. Then, r-PVC/CFA pellets (r-PVC/CFA-P) were obtained, concluding the extrusion and pelleting process.

The r-PVC/CFA-P were added into the hopper of a parallel twin-screw extruder to be extruded, cooled, shaped, hauled, cut, and finally formed into an r-PVC/CFA composites (*X* is used to denote the CFA content in the r-PVC/CFA composites in the form of r-PVC/CFA-*X*). The rotational speeds of the screws in the extruder and dosing unit were set to 20 and 21.5 rpm, respectively. The speed of the haul-off unit was set to 1.565 m·min⁻¹. The pressure and temperature of the melt were 16.8 MPa and 179°C, respectively. The sectional temperatures of the extruder barrel were set to 160°C, 160°C, and 159°C. The temperature of the connecting area was set to 160°C. The sectional temperatures of the die were set to 203°C, 203°C, 191°C, and 204°C.

2.3 Testing and characterization

2.3.1 Thermal analysis

A NETZSCH STA 449 F3 comprehensive thermal analyzer (NETZSCH-Gerätebau GmbH, Germany) was used to perform the thermogravimetric analysis (TGA). The testing range and heating rate were set to $30-1,000^{\circ}\text{C}$ and $10^{\circ}\text{C}\cdot\text{min}^{-1}$, respectively. N_2 was used as a protective gas. In addition, a Q20 differential scanning calorimeter (TA Instruments, USA) was used for differential scanning calorimetry measurements. The testing range and heating rate were set to $30-180^{\circ}\text{C}$ and $10^{\circ}\text{C}\cdot\text{min}^{-1}$, respectively. N_2 was used as a protective gas.

2.3.2 Mechanical analysis

A UTM4304 electronic universal testing machine (Shenzhen Suns Technology Stock Co., Ltd, China) was used to test the tensile and bending strengths of the specimens according to the GB1040.2-2006 and GB/T9341-2000 standards, respectively. I-shaped specimens were used for tensile strength testing (tensile speed: $2\,\mathrm{mm\cdot min^{-1}}$). Specimens having dimensions of $80\,\mathrm{mm}\times10\,\mathrm{mm}\times4\,\mathrm{mm}$ were used for the bending strength testing (span: $64\,\mathrm{mm}$ and speed: $2\,\mathrm{mm\cdot min^{-1}}$). An MZ-2056 cantilever beam impact testing machine (Jiangsu Mingzhu Testing Machinery Co., Ltd, China) was used to test specimens with a dimension of $80\,\mathrm{mm}\times10\,\mathrm{mm}\times4\,\mathrm{mm}$ following the GB/T1843-2008 standard. An HRS-150

digital Rockwell hardness machine (Shanghai Lianer Test Equipment Co., Ltd, China) was used to measure the hardness of the specimens. Each specimen had a thickness of 6 mm and an area large enough for measurements to be taken at a minimum of five points with a spacing of ≥ 10 mm and a distance of ≥ 10 mm from the closest edge of the specimen. A JM-101PT automatic nail-holding capacity tester for sheet materials was used to test specimens with dimensions of 150 mm \times 50 mm \times 50 mm at a speed of 2 mm·min⁻¹ according to the GB/T14018-2009 standard. Ordinary low-carbon steel nails with a length of 45 mm and a diameter of 2.5 mm were used in the test.

2.3.3 Other characterization and properties testing

The water absorption rates were tested according to the GB/T1034-2008 standard. The sample densities were tested using the immersion method according to the GB/T1033.1-2008 standard. The particle sizes were determined using a ×100 particle-size distribution analyzer (Beijing Honeywell Automatic Equipment Co., Ltd, China). Water was used as the dispersed phase, and the specimens were ultrasonically treated for 10 min before analysis. A WQF-520A Fourier-transform infrared spectroscopy system (Beijing Beifen-Ruili Analytical Instrument (Group) Co., Ltd, China) was used to analyze the functional groups in the samples. The samples were mixed with KBr and pressed into disks, and measurements were carried out between 500 and 4,000 cm⁻¹.

A full range dynamic contact angle meter (Shanghai Zhongchen Digital Technic Apparatus Co., Ltd, China) was used to test specimens. First, we placed the sample in the groove on a glass plate, pressed it, then the contact angle measurements were carried out. A SIGMA 500 scanning electron microscopy (SEM) system (Zeiss, Germany) was used to perform cross-sectional morphological analysis of the composite specimens. Each composite specimen was coated with gold before testing.

3 Results and discussion

3.1 CFA modification and characterization

The presence of surface hydroxyl groups makes CFA hydrophilic and reduces its compatibility with hydrophobic organic resins (Figure 2). Therefore, the surface modification of CFA is required before it can be used as a filler. In our process, the CFA is modified *in situ* during



Figure 2: Schematic of the CFA modification process.

mixing, which is superior to previous methods that require a multistep treatment and transport process; thus, our method produces less dust pollution in workshops than do conventional methods, rendering it practical for realworld applications.

As shown in Figure 3a, the CFA had a wide particlesize distribution, ranging from 0.55 to 65.06 µm. The median particle size (D_{50}) of the CFA particles was 10.46 µm. With relatively smooth surfaces, the CFA particles were irregular in shape and comprised mostly spherical particles; however, there were also some very large rod-like particles. The surface of the CFA modified by the aluminate coupling agent was rough, as shown in Figure 3b; however, the modification process did not alter the morphology of the CFA particles.

Figure 3c and d shows the contact angles of the CFA and modified CFA, respectively (static results of five measurements). As shown, a water film was formed on the surface of the CFA because of its high hydrophilicity [46]. In contrast, the modified CFA was very hydrophobic, as shown by its contact angle of $134 \pm 2^{\circ}$, which is a result of its organophilicity because of the presence of a layer of organic molecules on its surface after the aluminateinduced activation and modification [46-48].

Figure 4a shows the infrared spectra of the CFA, modified CFA, and aluminate. The characteristic peak of CFA at 1,103 cm⁻¹ can be attributed to the -Si-Ostretching vibrations of SiO₂ [49]. The spectrum of aluminate reveals the characteristic absorption peaks of -CH₂groups at 2,917 and 2,850 cm $^{-1}$ and those of -C=0 groups

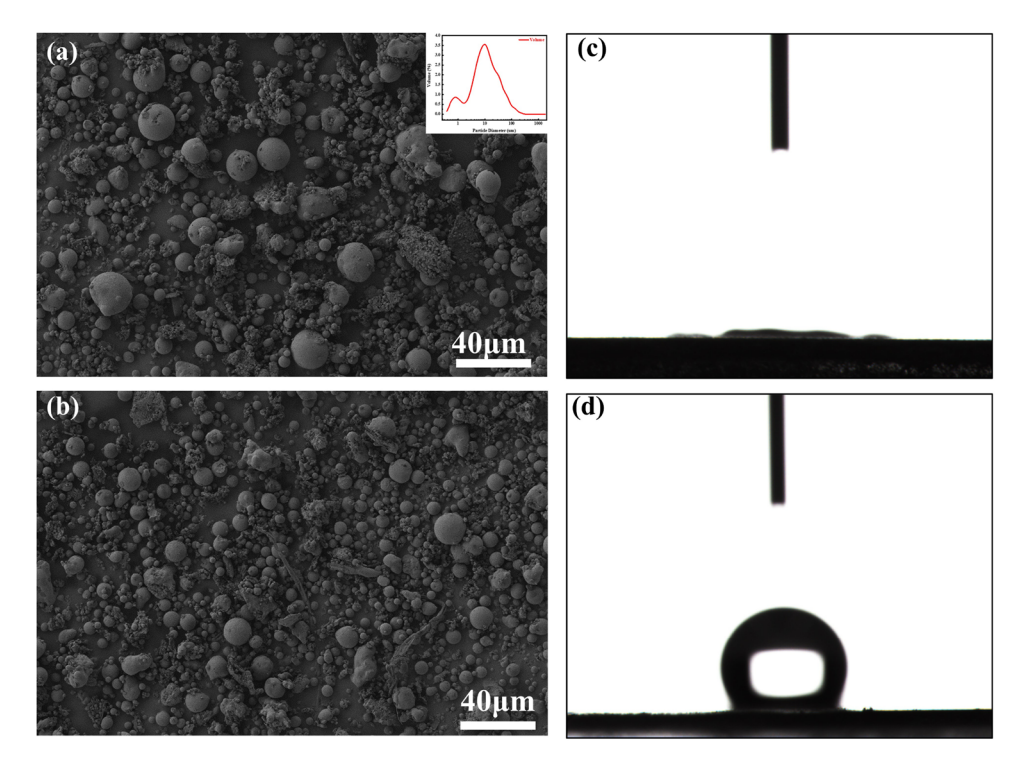


Figure 3: SEM images of (a) CFA particles and (b) modified CFA particles (inset in (a) is the particle-size distribution). Contact angle measurements for (c) CFA and (d) modified CFA.

6 — Zhaoshuai Li et al. DE GRUYTER

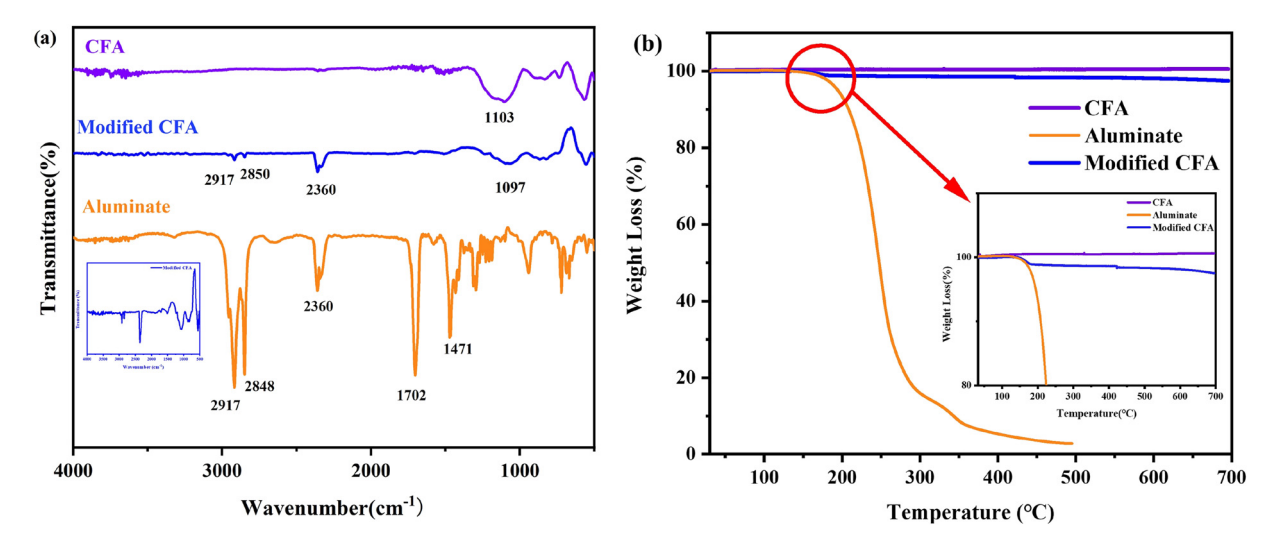


Figure 4: (a) FTIR spectra of CFA, modified CFA, and aluminate. (b) TGA profiles of CFA, modified CFA, and aluminate.

at $1,702 \, \text{cm}^{-1}$ [50,51]. In the IR spectrum of the modified CFA, the characteristic absorption peaks of $-\text{CH}_2$ – appear at $2,917 \, \text{and} \, 2,850 \, \text{cm}^{-1}$, whereas the characteristic absorption peak at $2,360 \, \text{cm}^{-1}$ can be ascribed to the interference from CO_2 , suggesting that the CFA had been modified satisfactorily.

Figure 4b shows the TGA profiles of the CFA, modified CFA, and aluminate. The weight of the CFA remained almost unchanged when heated to 700°C [49], whereas the modified CFA lost 1.4% of its weight when heated to 700°C. In contrast, the aluminate was almost completely degraded at 500°C, leaving only a trace amount of inorganic substances. Thus, the TGA results indicate that the degradation temperature of the modified CFA is consistent with that of aluminate. Therefore, the weight loss of the

modified CFA can be attributed to the degradation of aluminate.

3.2 Characterization of the r-PVC/CFA (r-PVC/CFA-X) composites

3.2.1 Effects of CFA content on the morphology of the r-PVC/CFA composites

As shown in Figure 5a, the r-PVC/CFA composites containing 80 phr of the unmodified CFA is poorly shaped and has a rough surface containing a large number of cracks. Figure 6a shows the corresponding micromorphology.

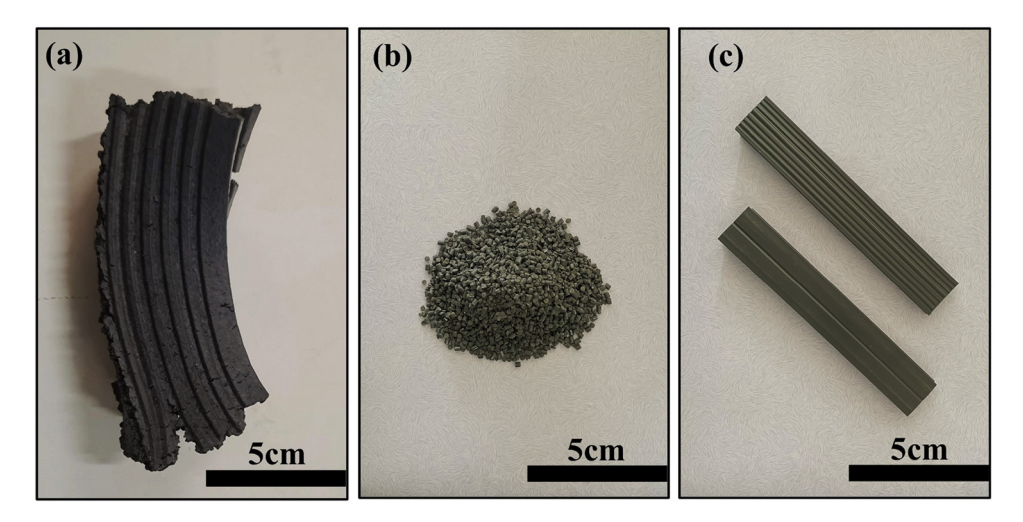


Figure 5: Macroscopic images of (a) unmodified r-PVC/CFA composites, (b) modified r-PVC/CFA-P, and (c) modified r-PVC/CFA composites.

As shown, the unmodified CFA was poorly compatible with the r-PVC resin, and there was a pronounced interfacial separation. In contrast, the r-PVC/CFA composites containing 80 phr of modified CFA has a smooth surface devoid of depressions and discoloration resulting from degradation (Figure 5c). Figure 6e shows the corresponding micromorphology. These morphological characteristics can be ascribed to the enhanced interfacial interactions of the modified CFA with the r-PVC resin. Promisingly, this result suggests that the DWSF produced from the composites would be suitable for commercial applications. However, increasing the CFA content caused considerably more CFA particles to fall off and some CFA particles to agglomerate, as shown in Figure 6f, which can be attributed to the decrease in the dispersion and uniformity of the CFA in the r-PVC resin with increase in the CFA content.

3.2.2 Effects of CFA content on the thermal degradation behavior of the r-PVC/CFA composites

Analysis of the TGA and derivative thermogravimetry (DTG) curves reveals two typical stages during the thermal degradation of the r-PVC. A first mass loss, denoted W_1 , which can be attributed to the loss of -Cl from the r-PVC chains and the formation of HCl gas and loss of -C=C-[52,53], and a second mass loss, denoted W_2 , which corresponds to the pyrolysis and degradation of the PVC chains after the elimination of HCl. In this step, the main chain of the polymer is mineralized into CO_2 and water [35].

As shown in Figure 7a–f, the TG–DTG curves show an upward trend at 0–230°C, possibly because of the high $\rm N_2$ flow rate or the small sample weight. As shown in Figure 7a, W_1 , W_2 , and W for r-PVC were 43.0%, 25.9%, and 68.9%, respectively, because CaCO₃ formed part of the r-PVC as a filler; in contrast, those of r-PVC/CFA-P (Figure 7b) were 19.2%, 19.4%, and 38.6%, respectively (Table 3), suggesting a relatively small mass loss. As shown in Figure 7c–f, as the CFA content increased, the mass loss of the composites gradually decreased, and this is a result of the increase in the inorganic filler content as a result of the introduction of the modified CFA into the r-PVC.

Analysis of the TG and DTG curves revealed that the temperatures corresponding to the maximum mass losses (T_1 and T_2 , respectively) of r-PVC in stages 1 and 2 were 296°C and 478°C, respectively. In contrast, those of the r-PVC/CFA composite pellets were 272°C and 458°C, respectively (Figure 7b; Table 3). As shown in Figure 7c-f, the T_1 and T_2 values for the r-PVC/CFA composites with a CFA content of 40 phr (i.e., r-PVC/CFA-40) were 276°C and 459°C, respectively. As the CFA content increased, both T_1 and T_2 for the r-PVC/CFA composites gradually increased, and the maximum values (286°C and 474°C, respectively) were obtained at a CFA content of 60 phr (i.e., r-PVC/CFA-60). Further increasing the CFA content did not significantly change T_1 and T_2 (Table 3).

Therefore, the addition of the modified CFA reduced the T_1 for the r-PVC/CFA composites, indicating a reduction in its thermal stability. This behavior can be explained as follows: SiO₂ and Al₂O₃ are the main chemical components

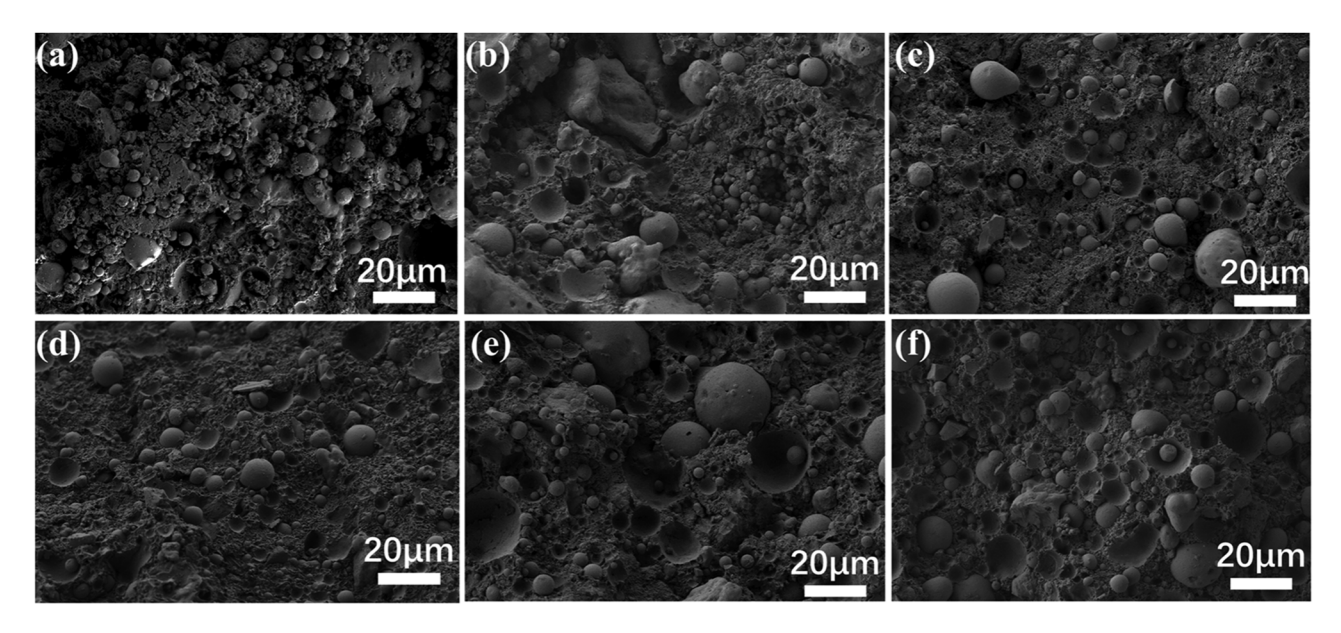


Figure 6: SEM images of (a) unmodified r-PVC/CFA composites, (b) modified r-PVC/CFA-P (80 phr CFA), and (c)–(f) r-PVC/CFA-X composites varied with X (40, 60, 80, and 100).

8 — Zhaoshuai Li et al. DE GRUYTER

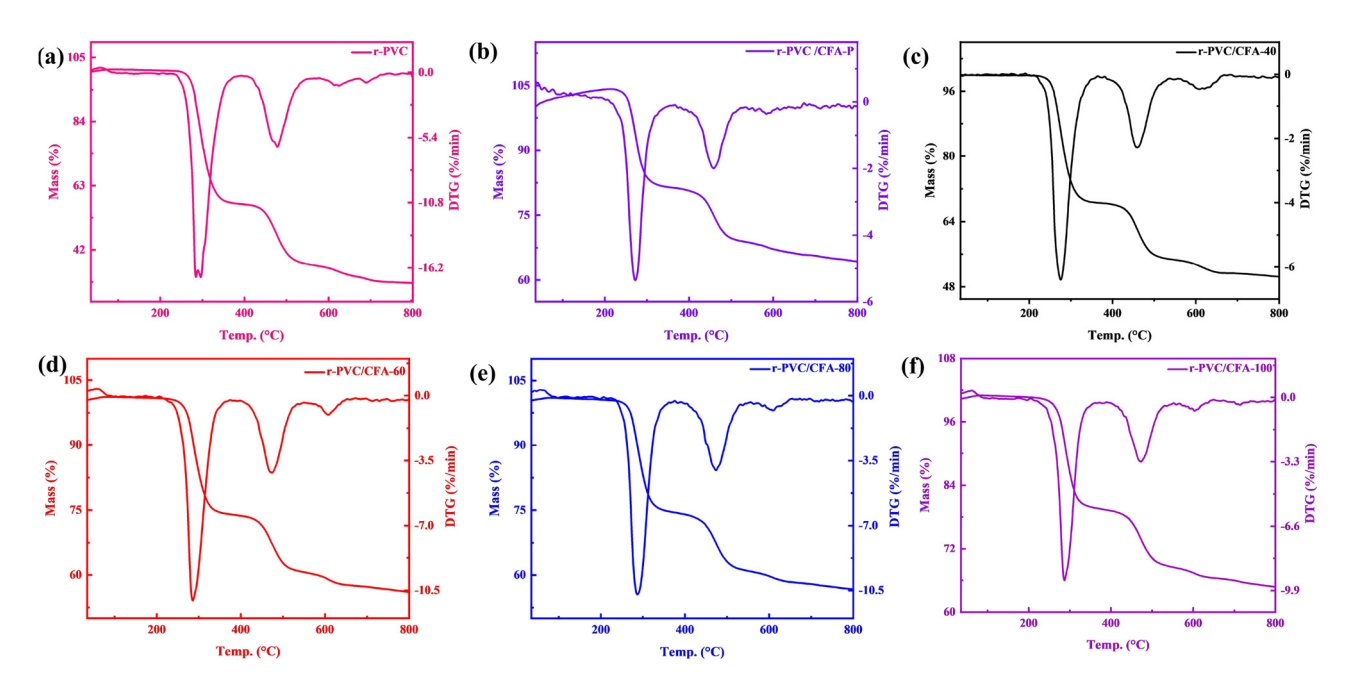


Figure 7: TGA and DTG curves for (a) r-PVC, (b) r-PVC/CFA-P composites (80 phr CFA), and (c-f) r-PVC/CFA-X composites varied with X (40, 60, 80, and 100).

of CFA and are solid acids that can catalyze the dechlorination of PVC. In addition, CFA also contains basic metal oxides (e.g., CaO, K_2O , and Na_2O), which have a high absorption capacity for HCl. As a result, CFA facilitates the elimination of HCl from the PVC matrix [35,54].

3.2.3 Effects of CFA content on the glass-transition temperature ($T_{\rm g}$) of the r-PVC/CFA composites

As shown in Figure 8, the $T_{\rm g}$ values of the r-PVC and r-PVC/CFA composites were 84.8°C and 82.3°C, respectively, and the $T_{\rm g}$ of the composites reached 77.6°C and 83.4°C at CFA contents of 80 and 100 phr, respectively. Therefore, the $T_{\rm g}$ of the composites was lower than that of r-PVC, which can be explained as follows. The addition of

a certain amount of additives (ACR and CPE) during preparation plasticized the PVC, to some extent and, thus, reduced its $T_{\rm g}$. However, the decrease in $T_{\rm g}$ does not affect the serviceability of the r-PVC/CFA composites.

3.2.4 Effects of CFA content on the mechanical properties of the r-PVC/CFA composites

The mechanical properties of the r-PVC/CFA composites developed in this study – a new type of r-PVC/CFA composites are crucial (Table 4). As shown in Figure 9, the impact strength of the r-PVC/CFA composites decreased significantly at a CFA content ≤ 80 phr, and the maximum impact strength (40.5 kJ·m⁻²) of the r-PVC/CFA composites was achieved at a CFA content of 40 phr. Increasing

Table 3: Thermal properties of the r-PVC, r-PVC/CFA-P, and r-PVC/CFA composites

Sample	First step		Secon	ıd step	W (%)	T_{g} (°C)
	<i>T</i> ₁ (°C)	W ₁ (%)	7 ₂ (°C)	W ₂ (%)		
r-PVC	296	43.0	478	25.9	68.9	84.8
r-PVC/CFA-P	272	19.2	458	19.4	38.6	82.3
r-PVC/CFA-40	276	31.6	459	18.0	49.6	78.3
r-PVC/CFA-60	286	26.3	474	17.7	44.0	80.9
r-PVC/CFA-80	285	25.6	472	17.2	42.8	77.6
r-PVC/CFA-100	287	20.7	473	14.6	35.3	83.4

 T_1 : temperature corresponding to the maximum mass loss in the first stage; T_2 : temperature corresponding to the maximum mass loss in the second stage; W_1 : mass loss of the first stage; W_2 : mass loss of the second stage; W: total mass loss.

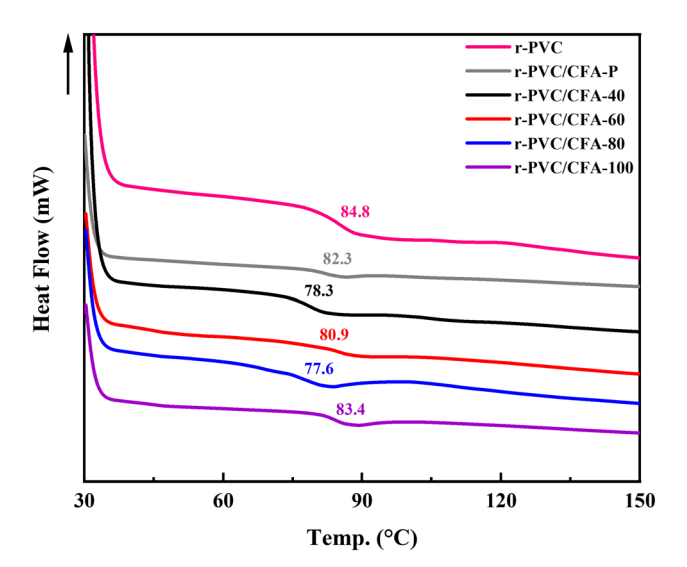


Figure 8: TGA curves for r-PVC, r-PVC/CFA-P, and r-PVC/CFA-X composites.

the CFA content beyond 80 phr caused almost no significant change in the impact strength of the r-PVC/CFA composites. At a CFA content of 100 phr, the impact strength of the r-PVC/CFA composites reached its minimum value of $10.1\,\mathrm{kJ\cdot m^{-2}}$, which is 75.1% lower than that at a CFA content of 40 phr. This can be explained as follows: the modified CFA was present mostly as spherical particles with a low aspect ratio that were somewhat "agglomerated," weakening the interfacial interaction between the r-PVC and CFA, which in turn led to a decrease in the impact strength of the composites.

Figure 9b and d shows the bending strength with respect to CFA content and the stress-strain curves, respectively. As shown, the bending strength decreased with increase in CFA content, and the bending strength reached its maximum (36.24 MPa) at a CFA content of 40 phr and minimum (25.6 MPa [29.4% lower than the maximum]) at a CFA content of 100 phr. Comparison of these values with industrial standards (bending strength: 31.6 MPa and bending modulus: \geq 2,400 MPa) suggests that a CFA content of 80 phr, which yielded a bending strength of 33 MPa, is optimal. The decrease in the bending strength of the r-PVC/CFA composites can be attributed to the following factors. Increasing the CFA

content reduced the dispersion of the CFA in the r-PVC resin and caused its partial agglomeration. Therefore, there are gaps between the CFA microspheres and r-PVC resin, which reduces the interfacial interaction between the CFA particles and PVC resin and increases the susceptibility of the composites to fracture on loading. In contrast, the bending modulus of the r-PVC/CFA composites increased as the CFA content increased. As a rigid particulate filler, CFA had a binding effect on the surrounding r-PVC. Thus, the addition of CFA restricted the chain mobility, thereby increasing the bending modulus.

As shown in Figure 9c, as the CFA content increased, the Rockwell hardness of the r-PVC/CFA composites first increased and then decreased. In particular, as the CFA content increased from 40 to 60 phr, the Rockwell hardness did not change significantly, decreasing from 72 to 68. However, on increasing the CFA content from 40 to 80 phr, the Rockwell hardness increased by 23.9%, reaching a maximum of 89.2, probably as a result of the high hardness of CFA. As the CFA content increased from 80 to 100 phr, the Rockwell hardness of the composites decreased by 13.7% to 77 because of the uneven loading caused by the less uniform dispersion of CFA in the r-PVC resin with increase in CFA content.

Combining the above results, the optimal CFA content is 80 phr (i.e., r-PVC/CFA-80 was the optimum composites). Subsequent testing of the r-PVC/CFA-80 composites revealed that it has a density of $1.73~\rm g\cdot cm^{-3}$ (industrial standard: ≤ 1.8 and $\geq 1.35~\rm g\cdot cm^{-3}$), tensile strength of $13.6~\rm MPa$, nail-holding capacity of $4,800~\rm N$ (industrial standard: $\geq 3,000~\rm N$), and $24~\rm h$ water absorption rate of 0.3% (industrial standard: $\leq 0.5\%$). These metrics either match or are better than those of the corresponding industrial standards, suggesting that the r-PVC/CFA-80 composites have potential for commercial applications.

3.3 Economic assessment of traditional and new sub-frame materials

As shown in Figure 10 and Table 2, the conventional DWSF material is fabricated via the extrusion and

Table 4: Mechanical properties of r-PVC/CFA composites

Sample	Bending strength (MPa)	Bending modulus (MPa)	Impact strength (kJ·m ⁻²)	Hardness (HRR)	
r-PVC/CFA-40	36.24	3,609	40.5	72.0	
r-PVC/CFA-60	34.10	3,953	27.5	68.0	
r-PVC/CFA-80	33.00	4,188	11.1	89.2	
r-PVC/CFA-100	25.60	4,352	10.1	77.0	

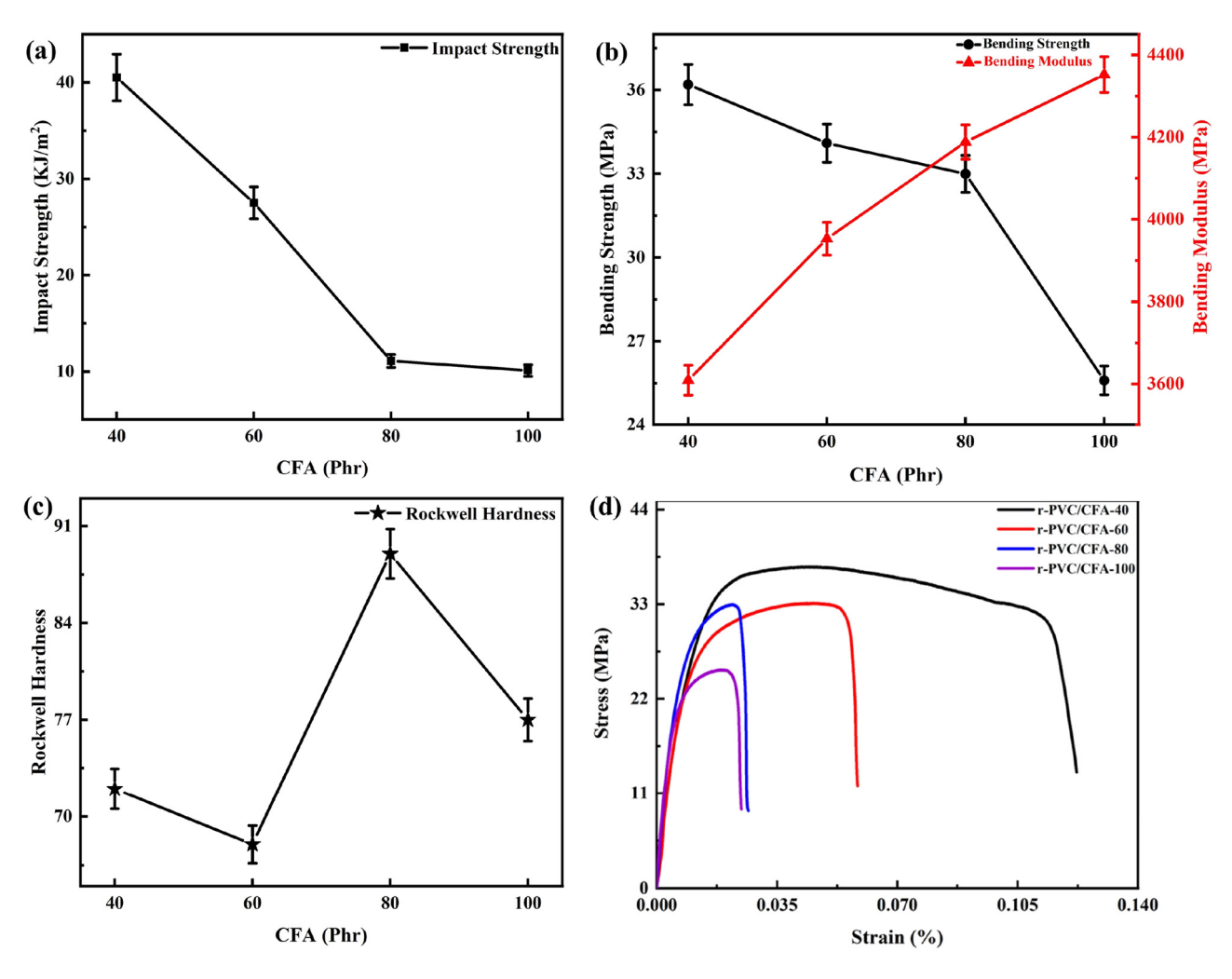


Figure 9: (a) Impact properties of r-PVC/CFA-X composites, (b) r-PVC/CFA-X composites flexural strength and flexural modulus, (c) Rockwell hardness of r-PVC/CFA-X composites, and (d) bending strength stress—strain of r-PVC/CFA-X composites.

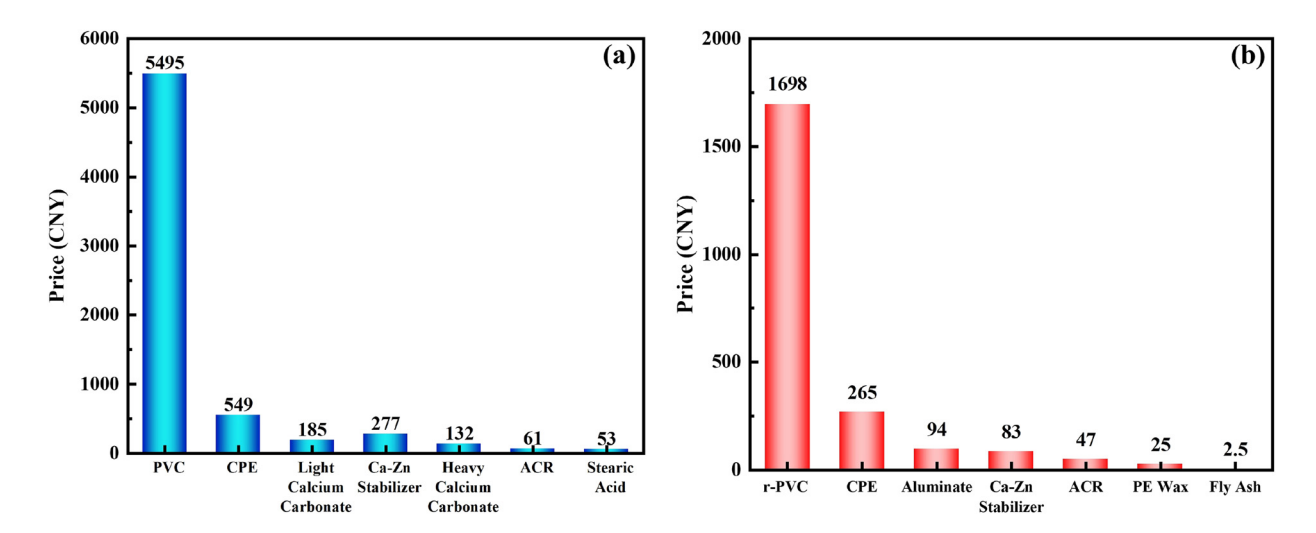


Figure 10: Production of per ton composites cost estimates: (a) traditional CaCO₃-based DWSF composites and (b) new CFA-based DWSF composites.

shaping of a mixture of light and heavy CaCO₃ (filler), PVC (raw materials), and additives. The prices for PVC, r-PVC, light CaCO₃, and heavy CaCO₃ are 10,000, 1,100, and 450 CNY/ton, respectively. In contrast, CFA and r-PVC are the raw materials for the r-PVC/CFA composites, the prices of CFA and r-PVC are 6 and 3,200 CNY/ton, respectively. Therefore, the use of CFA and r-PVC appreciably reduces the production cost per ton of DWSF by 20-35%. Furthermore, combined with our recipes table (Table 2) we arrive at the conclusion that replacing CaCO3 with modified CFA as a filler to fabricate new DWSF composites will consumes ca. 424 kg CFA and 530 kg r-PVC per ton. Therefore, our CFA-based DWSF production approach offers significant economic benefits and social benefits.

4 Conclusion

In summary, we developed a new process to reuse second resources CFA and r-PVC to produce DWSF composite materials. The hot-mixing of CFA with aluminate in onepot realized CFA in situ modification and improved its compatibility with r-PVC. Crucially, this one-step process prevents dust pollution (a potential problem associated with the conventional multistep procedures), thereby protecting the environment and the health of the workers. The effectiveness of the strategy was demonstrated through careful characterization of the physical properties of the composites, which exhibited exceptional mechanical performance. Critically, the bending strength and modulus, impact strength, hardness, and waterproof performance of the obtained DWSF composite materials comply with the current industrial standards. As our process is rather simple and robust, it was industrialized. More importantly, according to our strategy to produce DWSF, it is estimated that the production cost is reduced by about 20-35% and consumes 424 kg CFA and 530 kg r-PVC per ton, which presents rather significant economic benefits and social benefits.

Funding information: This work was supported by Key Research and Development Program of Ningxia (Grant Nos. 2022BDE02001 and 2022BDE03003), Fundamental Research Funds for the Central Universities, North Minzu University (Grant No. 2020KYQD32), Key Research and Development Program (Talents Project) of Ningxia (Grant No. 2021BEB04067), the Natural Science Foundation of Ningxia (Grant No. 2022AAC03220), and the Science and Technology Innovation Project of Yinchuan (Grant No. 2022ZDGX11).

Author contributions: Zhaoshuai Li: writing - original draft, investigation, formal analysis; Jun Yan and Yonggiang Qian: writing - review and editing, formal analysis; Shengwei Guo and Yuan Liu: writing – review and editing, investigation; Guxia Wang and Dan Li: conceptualization, methodology, funding acquisition, writing - review and editing.

Conflict of interest: Authors state no conflict of interest.

References

- Luo Y, Wu Y, Ma S, Zheng S, Zhang Y, Chu PK. Utilization of coal fly ash in China: a mini-review on challenges and future directions. Environ Sci Pollut R. 2021;28(15):18727-40. doi: 10.1007/s11356-020-08864-4.
- Feng W, Wan Z, Daniels J, Li Z, Xiao G, Yu J, et al. Synthesis of high quality zeolites from coal fly ash: mobility of hazardous elements and environmental applications. J Clean Prod. 2018;202:390-400. doi: 10.1016/j.jclepro.2018.08.140.
- [3] Wang H, Wang M, Zhang J, Wang N, Wang J, Yang J. Preparation of fly ash-based cobalt-iron silicate as supercapacitor electrode material. Chem Eng J. 2022;434:134661. doi: 10.1016/j. cej.2022.134661.
- Zeng Z, Wei Y, Wei Z, Yao W, Wang C, Huang B, et al. Deep learning enabled particle analysis for quality assurance of construction materials. Autom Constr. 2022;140(4):104374. doi: 10.1016/j.autcon.2022.104374.
- Wang D, Wan K, Yang J. Measurement and evolution of ecoefficiency of coal industry ecosystem in China. J Clean Prod. 2019;209:803-18. doi: 10.1016/j.jclepro.2018.10.266.
- Hwang S, Jin SH, Kim Y, Seo JS, So J-I, Kim J, et al. Deciphering van der Waals interaction between polypropylene and carbonated fly ash from experimental and molecular simulation. J Hazard Mater. 2022;421:126725. doi: 10.1016/j.jhazmat. 2021.126725.
- Huang Y, Zheng X, Wei Y, He Q, Yan S, Ji L. Protonated amines mediated CO₂ mineralization of coal fly ash and polymorph selection of CaCO₃. Chem Eng J. 2022;450:138121. doi: 10.1016/j.cej.2022.138121.
- [8] Chen H, Chen Q, Xu Y, Lawi AS. Effects of silica fume and fly ash on properties of mortar reinforced with recycled-polypropylene. Constr Build Mater. 2022;316:125887. doi: 10.1016/j. conbuildmat.2021.125887.
- Zhan X, Kirkelund GM. Electrodialytic remediation of municipal solid waste incineration fly ash as pre-treatment before geopolymerisation with coal fly ash. J Hazard Mater. 2021;412:125220. doi: 10.1016/j.jhazmat.2021.125220.
- Ma L, Feng Y, Zhang M, Zheng Q, Wang B, Han L, et al. Mechanism study on green high-efficiency hydrothermal activation of fly ash and its application prospect. J Clean Prod. 2020;275:122977. doi: 10.1016/j.jclepro.2020.122977.
- [11] Lin C-Y, Chen T-A. Effects of composition type and activator on fly ash-based alkali activated materials. Polymer. 2021;14(1):63. doi: 10.3390/polym14010063.
- [12] Luo Y, Tian J, Liu C, Wu Y. Distinction between lignite fly ash and high-alumina fly ash: a thorough comment. Sci Total

- Environ. 2021;757:142990. doi: 10.1016/j.scitotenv.2020. 142990.
- [13] Doddamani M. Dynamic mechanical analysis of 3D printed eco-friendly lightweight composite. Compos Commun. 2020;19:177-81. doi: 10.1016/j.coco.2020.04.002.
- [14] Wang X, Fu C, Feng Z, Huo H, Yin X, Gao G, et al. Flyash/polymer composite electrolyte with internal binding interaction enables highly-stable extrinsic-interfaces of all-solid-state lithium batteries. Chem Eng J. 2022;428:131041. doi: 10.1016/j.cej.2021.131041.
- [15] Xue Y, Liu X. Detoxification, solidification and recycling of municipal solid waste incineration fly ash: a review. Chem Eng J. 2021;420:130349. doi: 10.1016/j.cej.2021.130349.
- [16] Turgut P, Demir F. The influence of disposed fly ash on Ca²⁺ leaching and physico-mechanical properties of mortars. J Clean Prod. 2019;226:270–81. doi: 10.1016/j.jclepro.2019.04.105.
- [17] Teixeira ER, Camoes A, Branco FG, Aguiar JB, Fangueiro R. Recycling of biomass and coal fly ash as cement replacement material and its effect on hydration and carbonation of concrete. Waste Manage. 2019;94:39–48. doi: 10.1016/j.wasman. 2019.05.044.
- [18] Nguyen TBT, Chatchawan R, Saengsoy W, Tangtermsirikul S, Sugiyama T. Influences of different types of fly ash and confinement on performances of expansive mortars and concretes. Constr Build Mater. 2019;209:176–86. doi: 10.1016/j. conbuildmat.2019.03.032.
- [19] Bellum RR. Influence of steel and PP fibers on mechanical and microstructural properties of fly ash-GGBFS based geopolymer composites. Ceram Int. 2022;48(5):6808–18. doi: 10.1016/j. ceramint.2021.11.232.
- [20] Zhou L, Zheng Y, Yu Y, Song G, Huo L, Guo Y. Experimental study of mechanical and fresh properties of HVFA-SCC with and without PP fibers. Constr Build Mater. 2021;267:121010. doi: 10.1016/j.conbuildmat.2020.121010.
- [21] Gadore V, Ahmaruzzaman M. Tailored fly ash materials: a recent progress of their properties and applications for remediation of organic and inorganic contaminants from water. J Water Process Eng. 2021;41:101910. doi: 10.1016/j. jwpe.2020.101910.
- [22] Yao ZT, Ji XS, Sarker PK, Tang JH, Ge LQ, Xia MS, et al. A comprehensive review on the applications of coal fly ash. Earth-Sci Rev. 2015;141:105–21. doi: 10.1016/j.earscirev.2014. 11.016.
- [23] Xin BP, Jiang WF, Aslam H, Zhang K, Liu CH, Wang RQ, et al. Bioleaching of zinc and manganese from spent Zn-Mn batteries and mechanism exploration. Bioresour Technol. 2012;106:147-53. doi: 10.1016/j.biortech.2011.12.013.
- [24] Lu C-F, Wang W, Li Q-T, Hao M, Xu Y. Effects of micro-environmental climate on the carbonation depth and the pH value in fly ash concrete. J Clean Prod. 2018;181:309–17. doi: 10.1016/ j.jclepro.2018.01.155.
- [25] Ahmaruzzaman M. A review on the utilization of fly ash. Prog Energ Combust. 2010;36(3):327–36. doi: 10.1016/j.pecs.2009. 11.003.
- [26] Chu Y-S, Davaabal B, Kim D-S, Seo S-K, Kim Y, Ruescher C, et al. Reactivity of fly ashes milled in different milling devices. Rev Adv Mater Sci. 2019;58(1):179–88. doi: 10.1515/rams-2019-0028.
- [27] Barman P, Singh B. Strength characteristics of sand amended with two waste materials fly ash and scrap tyre. Environ

- Process. 2019;7(2):653-72. doi: 10.1007/s40710-019-00412-8.
- [28] Sun Q, Tian S, Sun Q, Li B, Cai C, Xia Y, et al. Preparation and microstructure of fly ash geopolymer paste backfill material. J Clean Prod. 2019;225:376–90. doi: 10.1016/j.jclepro.2019. 03.310.
- [29] Sevim Ö, Demir İ. Physical and permeability properties of cementitious mortars having fly ash with optimized particle size distribution. Cem Concr Compos. 2019;96:266–73. doi: 10.1016/j.cemconcomp.2018.11.017.
- [30] Choo H, Won J, Burns SE. Thermal conductivity of dry fly ashes with various carbon and biomass contents. Waste Manage. 2021;135:122-9. doi: 10.1016/j.wasman.2021.08.033.
- [31] Shi Y, Li Y, Tang Y, Yuan X, Wang Q, Hong J, et al. Life cycle assessment of autoclaved aerated fly ash and concrete block production: a case study in China. Environ Sci Pollut R. 2019;26(25):25432–44. doi: 10.1007/s11356-019-05708-8.
- [32] Wang L, Sun H, Sun Z, Ma E. New technology and application of brick making with coal fly ash. J Mater Cycles Waste. 2015;18(4):763-70. doi: 10.1007/s10163-015-0368-9.
- [33] Qi L, Xu J, Liu K. Porous sound-absorbing materials prepared from fly ash. Environ Sci Pollut R. 2019;26(22):22264-72. doi: 10.1007/s11356-019-05573-5.
- [34] Czarna-Juszkiewicz D, Cader J, Wdowin M. From coal ashes to solid sorbents for hydrogen storage. J Clean Prod. 2020;270:122355. doi: 10.1016/j.jclepro.2020.122355.
- [35] Xiu F-R, Yu X, Qi Y. A high-efficiency and low-temperature subcritical water dechlorination strategy of polyvinyl chloride using coal fly ash (CFA) and coal gangue (CG) as enhancers. J Clean Prod. 2020;260:121085. doi: 10.1016/j.jclepro.2020. 121085.
- [36] Bora PJ, Porwal M, Vinoy KJ, Ramamurthy PC, Madras G. Industrial waste fly ash cenosphere composites based broad band microwave absorber. Compos Part B-Eng. 2018;134:151–63. doi: 10.1016/j.compositesb.2017.09.062.
- [37] Atun G, Ayar N, Kurtoglu AE, Ortaboy S. A comparison of sorptive removal of anthraquinone and azo dyes using fly ash from single and binary solutions. J Hazard Mater. 2019;371:94–107. doi: 10.1016/j.jhazmat.2019.03.006.
- [38] Zaichenko NM, Nefedov VV. Poly (ethylene terephthalate) composite material with modified fly ash filler. Mag Civ Eng. 2021;101(1):10103. doi: 10.34910/MCE.101.3.
- [39] Nath S, Jena H, Priyanka, Sahini D. Analysis of mechanical properties of jute epoxy composite with cenosphere filler. Silicon-Neth. 2019;11(2):659-71. doi: 10.1007/s12633-018-9941-x.
- [40] Kumar M, Sahoo S, Surekha B, Sahoo S. Study of mechanical property of cenosphere and clamshell as filler material in jute epoxy composite. Advances in Materials and Manufacturing Engineering. Singapore: Springer; 2020. p. 607–15. doi: 10.1007/978-981-15-1307-7_69.
- [41] Verma P, Kumar A, Chauhan SS, Verma M, Malik RS, Choudhary V. Industrially viable technique for the preparation of HDPE/fly ash composites at high loading: thermal, mechanical, and rheological interpretations. J Appl Polym Sci. 2017;45995:1–8. doi: 10.1002/app.45995.
- [42] Khoshnoud P, Abu-Zahra N. The effect of particle size of fly ash (FA) on the interfacial interaction and performance of PVC/FA composites. J Vinyl Addit Technol. 2019;25:134–43. doi: 10.1002/vnl.21633.

- [43] Gohatre OK, Biswal M, Mohanty S, Nayak SK. Study on thermal, mechanical and morphological properties of recycled poly(vinyl chloride)/fly ash composites. Polym Int. 2020;69(6):552-63. doi: 10.1002/pi.5988.
- [44] Khoshnoud P, Wolgamott JC, Abu-Zahra N. Evaluating recyclability of fly ash reinforced polyvinyl chloride foams. J Vinyl Addit Technol. 2018;24(2):154-61. doi: 10.1002/vnl.21541.
- [45] Sim J, Kang Y, Kim BJ, Park YH, Lee YC. Preparation of fly ash/ epoxy composites and its effects on mechanical properties. Polymers-Basel. 2020;12(1):79. doi: 10.3390/polym12010079.
- [46] Jia Y, Feng H, Shen D, Zhou Y, Chen T, Wang M, et al. Highperformance microbial fuel cell anodes obtained from sewage sludge mixed with fly ash. J Hazard Mater. 2018;354:27-32. doi: 10.1016/j.jhazmat.2018.04.008.
- [47] Xue X, Liu Y-L, Dai J-G, Poon C-S, Zhang W-D, Zhang P. Inhibiting efflorescence formation on fly ash-based geopolymer via silane surface modification. Cem Concr Compos. 2018;94:43-52. doi: 10.1016/j.cemconcomp.2018.08.013.
- [48] Khan MZ, Baheti V, Militky J, Ali A, Vikova M. Superhydrophobicity, UV protection and oil/water separation properties of fly ash/trimethoxy(octadecyl)silane coated cotton fabrics. Carbohyd Polym. 2018;202:571-80. doi: 10.1016/j.carbpol.2018.08.145.

- [49] Van Der Merwe EM, Prinsloo LC, Mathebula CL, Swart HC, Coetsee E, Doucet FJ. Surface and bulk characterization of an ultrafine south african coal fly ash with reference to polymer applications. Appl Surf Sci. 2014;317:73-83. doi: 10.1016/j. apsusc.2014.08.080.
- [50] Patil AG, Anandhan S. Influence of planetary ball milling parameters on the mechano-chemical activation of fly ash. Powder Technol. 2015;281:151-8. doi: 10.1016/j.powtec.2015.04.078.
- Patil AG, Shanmugharaj AM, Anandhan S. Interparticle inter-[51] actions and lacunarity of mechano-chemically activated fly ash. Powder Technol. 2015;272:241-9. doi: 10.1016/j.powtec. 2014.12.006.
- [52] Wang Z, Xie T, Ning X, Liu Y, Wang J. Thermal degradation kinetics study of polyvinyl chloride (PVC) sheath for new and aged cables. Waste Manage. 2019;99:146-53. doi: 10.1016/j. wasman.2019.08.042.
- [53] Yu J, Sun L, Ma C, Qiao Y, Yao H. Thermal degradation of PVC: a review. Waste Manage. 2016;48:300-14. doi: 10.1016/j. wasman.2015.11.041.
- [54] Hapipi AM, Suda H, Uddin MA, Kato Y. Dechlorination of polyvinyl chloride under superheated steam with catalysts and adsorbents. Energ Fuel. 2018;32(7):7792-9. doi: 10.1021/acs. energyfuels.8b00838.